International Journal of Nanomedicine

Dovepress
Taylor & Francis Group

Open Access Full Text Article

ORIGINAL RESEARCH

Human Umbilical Cord Mesenchymal Stem Cells-Derived Exosomes Attenuates Experimental Periodontitis in Mice Partly by Delivering miRNAs

Ke Li[1], Xiaoli Gu[1], Yanan Zhu[1], Ning Guan[2], Jinlei Wang[3], Linyuan Wang[1]

[1]Department of Periodontics and Mucosa, The second Affiliated Hospital of Jinzhou Medical University, Jinzhou, Liaoning, 121000, People's Republic of China; [2]Key Laboratory of Brain and Spinal Cord Injury Research, First Affiliated Hospital of Jinzhou Medical University, Jinzhou, Liaoning, 121000, People's Republic of China; [3]School of Pharmacy, Jinzhou Medical University, Jinzhou, Liaoning, 121000, People's Republic of China

Correspondence: Linyuan Wang, Email wangly@jzmu.edu.cn

Introduction: Periodontitis is the most common non-communicable disease in humans. The main challenge in the treatment of periodontitis is to effectively control periodontal inflammation and promote tissue repair. Human umbilical cord mesenchymal stem cells-derived exosomes (hucMSCs-exo) have been reported to modulate inflammatory responses and promote tissue repairment mainly through miRNAs in several diseases. However, the effect of hucMSCs-exo on periodontitis remains unknown. In this study, we hypothesized that hucMSCs-exo could inhibit bone destruction in periodontitis mice.

Methods: In this study, we constructed and characterized the exo@H drug delivery platform. Lipopolysaccharide was used to construct an inflammatory microenvironment in vitro to detect MC3T3-E1 cells proliferation and bone regeneration capacity. Ligation induced to construct an experimental periodontitis mouse model. The distance of the cement-enamel junction (CEJ) to the alveolar bone crest (ABC) was measured for bone resorption evaluation. Hematoxylin-eosin (H&E) staining and Tartrate resistant acid phosphatase (TRAP) staining were used to observe periodontal tissue changes. MicroRNA (miRNA) sequencing was used to detect differential genes and for bioinformatics analysis. Real-time quantitative polymerase chain reaction (qRT-PCR). WB assay and dual luciferase assay were used to further validate the screened differentially expressed miRNAs and the targeted binding relationship with the corresponding target genes.

Results: We found that lyophilized hucMSCs-exo promoted the proliferation and osteogenic differentiation of MC3T3-E1 cells, and showed more significant proliferative and osteogenic differentiation abilities in combination with the hydrogel ($P < 0.05$). Using periodontitis mice, bone resorption evaluation revealed a significant reduction in alveolar bone resorption in the exo@H group compared to the hydrogel group ($P < 0.01$), and exo@H was able to reduce the inflammatory response of periodontal tissues and the number of osteoclasts on the surface of the alveolar bone compared to the hydrogel group. Moreover, 59 miRNAs were upregulated, such as let-7f-5p and miR-203-3p, which positively targeted IL-13 and Nit2, respectively.

Discussion: These results suggest that exo@H provides protection against periodontitis partly by delivering miRNAs to periodontal tissue. Our results confirm the feasibility of the exo@H delivery platform we constructed and the effectiveness of its use for periodontitis treatment, and this study provides a promising approach for the treatment of periodontitis via miRNA.

Keywords: periodontitis, exosomes, MC3T3-E1, microRNA, gene

Introduction

Periodontitis is a common clinical inflammatory disease of the oral cavity, characterized by the destruction of periodontal supporting tissues, and closely associated to systemic diseases.[1] It has been reported that globally, periodontitis has a prevalence of 20%-50%, making it the sixth most widespread disease in the general population.[2] The clinical treatments for periodontitis including mechanical plaque removal, regenerative surgical treatments, adjunctive laser treatments, and pharmacological treatments still suffer from the problems of timeliness and surgical complexity, and are particularly

Received: 11 November 2024
Accepted: 20 February 2025
Published: 8 March 2025

unsatisfactory in controlling periodontal inflammation while promoting tissue repair.[3] Therefore, it's crucial to seek new therapeutic strategies for periodontitis.

Exosomes are vesicles secreted by various cells, with a diameter ranging between 30–150 nm, and have structures and functions similar to the secreting cells,[4] enriched with various bioactive molecules like miRNA, mRNA, lipids, and proteins. Research indicates that in various disease models, exosomes secreted by MSCs can serve as an alternative therapy to MSCs paracrine actions, and offer compelling advantages compared to parental MSCs, such as no risk of tumor formation and concerns of immune rejection.[5] Some studies have shown that compared to exosomes from other cell sources, human umbilical cord mesenchymal stem cells-derived exosomes (hucMSCs-exo) have significant wound healing and tissue regeneration capabilities.[6,7] Moreover, they are easily harvested, avoiding the challenges associated with the shortage of embryonic stem cells and ethical constraints,[8] making them an ideal stem cell source in regenerative medicine.

MiRNAs are a group of small non-coding molecular RNAs consisting of 18–24 nucleotides, regulates gene expression by binding to the 3'UTR region of target genes.[9,10] Research has found that miRNA is a key functional carrier in exosomes.[11] Exosomes can carry numerous miRNAs, accounting for about 43% of the RNA in exosomes, these miRNAs can transfer genetic information, thereby inducing phenotypic changes in recipient cells and enhancing the therapeutic effects of MSCs-derived exosomes, playing a crucial role in the biological regulatory functions of exosomes.[12–14]

Exosome therapy is a promising approach for treating periodontitis, achieving therapeutic effects through the sustained release of miRNAs.[15] However, due to the rapid metabolism of exosomes, traditional exosome therapies mainly administer drugs through high doses and multiple injections, resulting in waste of exosomes and inconvenience and pain to patients.[16] Moreover, the high production costs of exosomes and their limited storage duration pose challenges. How to effectively preserve exosomes without losing their functional activity, and how to achieve targeted delivery of exosomes to affected areas while extending their retention time, are the two main challenges in utilizing exosomes for periodontitis treatment. Therefore, we employ the hydrogel with high biocompatibility, good biodegradability, and hydrophilicity to load the lyophilized hucMSCs-exo, creating a new bioactive scaffold to prevent their rapid clearance and optimizing the application of exosomes in the affected areas.[17]

The main components of the hydrogel are polyvinyl alcohol (PVA) and sodium alginate (Alg), PVA is a synthetic derivative of polyvinyl acetate with good biocompatibility, biodegradability, elasticity and hydrophilicity, which can be chemically or physically cross-linked to form the hydrogel.[18,19] Alg is a natural polysaccharide with the properties of stability, solubility, and safety required for excipients in drug preparation, etc.[20] PVA is able to strengthen the original mechanically weak alginate polymer, which makes the hydrogel obtained by cross-linking PVA and Alg through calcium ion is not only have good mechanical properties, biocompatibility and biodegradability, but also safe and stable It supports long-term cell viability and cell infiltration into the periodontal space, and can effectively solve the shortcomings of exosomes in terms of poor mechanical properties, low bioactivity, short action time and sudden release, and enhance the role of exosomes in promoting periodontal tissue regeneration.[21]

A previous study by our group found that hucMSCs-exo could accelerate diabetic wound healing by promoting angiogenesis.[22] We noted the potential of hucMSCs-exo in the treatment of periodontitis. In this study, our hypothesis suggests that hucMSCs-exo could attenuate periodontal inflammation and alveolar bone destruction in mice by regulating gene levels, as shown Scheme 1. By constructing a delivery system of hydrogel-loaded lyophilized hucMSCs-exo, elucidating the efficacy of the system on periodontitis using an animal model of periodontitis and in vitro cell culture, and further exploring the possible mechanism of action of hydrogel-loaded lyophilized hucMSCs-exo (exo@H) in affecting periodontitis from the perspective of miRNAs, we aim to provide a reference for the future clinical application of exo@H in periodontitis treatment.

Materials and Methods

Materials

Lyophilized hucMSCs-exo were provided by Shenyang Inno Medical Consulting Services Co., Ltd.; Mouse pre-osteoblastic cell line (MC3T3-E1 cells, Cell Bank of the Chinese Academy of Sciences, Shanghai); 3-(4,5-dimethylthiazol-2-yl)-2,5-diphenyltetrazolium bromide (MTT) were obtained from Beijing Dingguo Changsheng Biotechnology Co., Ltd.; Body

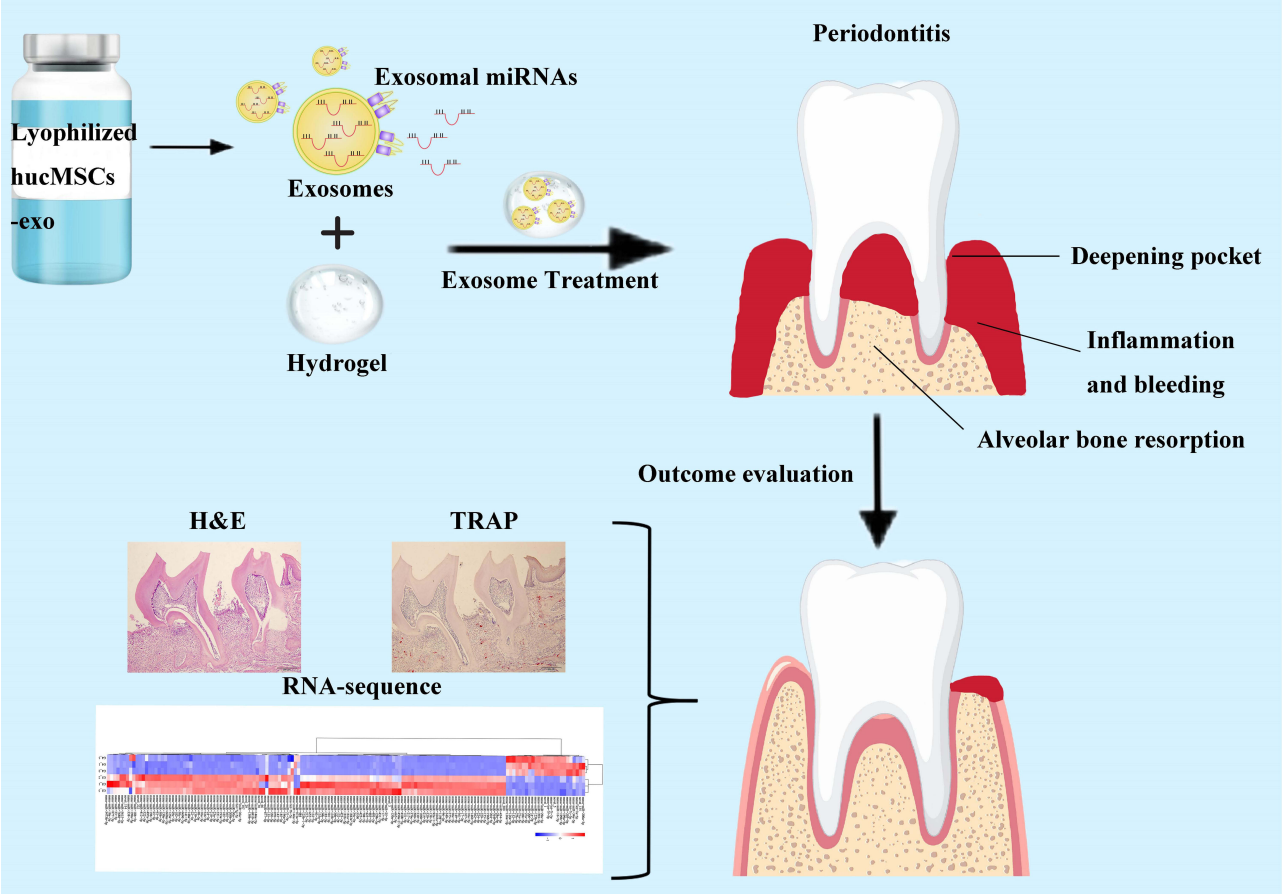

Scheme 1 Mechanism diagram of exo@H treatment for periodontitis. The hydrogel loaded with lyophilized hucMSCs-exo attenuated periodontal inflammation and inhibited bone resorption, partly by delivering miRNAs to modulate the expression of the corresponding genes.

vision microscope (Leica M165C, Germany); Three-dimensional cryo-mill (Wuhan Seville Biotechnology Co., Ltd).; Hematoxylin and eosin (H&E) staining kit (Beijing Solarbio Science & Technology Co., Ltd).; Lipopolysaccharide (LPS) (Beijing Solarbio Science & Technology Co., Ltd).; Tartrate-resistant acid phosphatase staining (TRAP staining kit) (Shanghai Beyotime Biotechnology Co., Ltd).; BCIP/NBT alkaline phosphatase color development kit and Alizarin Red S staining solution (0.2%, pH=8.3) were purchased from Biotium Biotechnology; IL-13 Antibody and Nit2 Antibody were purchased from Abmart Shanghai Co., Ltd.

Animals: C57BL/6 female mice (7 weeks old, weighing 18 g) were purchased from Liaoning Changsheng Biotechnology Co., Ltd., with a license number: SCXK (Liao) 2020–0001, and were bred in the SPF animal laboratory of Jinzhou Medical University. Mice were allowed free access to distilled water and standard food, as well as 12:12 h light-dark cycle. Animal experiments were conducted in accordance with the guidelines of the National Animal Society, including welfare and treatment of animals, and approved by the Animal Protection and Ethics Committee of Jinzhou Medical University, approval number: 2022101503.

Cell Culture

MC3T3-E1 cells were cultured in a medium containing 10% heat-inactivated fetal bovine serum (FBS) (Procell Life Science&Technology Co., Ltd., Wuhan), 1% penicillin-streptomycin (Gibco, Grand Island, USA) in a-MEM medium (Procell Life Science&Technology Co., Ltd., Wuhan), and cultured in an incubator at 37 °C with 95% humidity and 5% CO_2. Mineralization medium was prepared by adding 50 μg mL^{-1} ascorbic acid, 10 mm sodium β-glycerophosphate and

https://doi.org/10.2147/IJN.S502192

10 nM dexamethasone to a-MEM, with 2 d/change. Cells were stimulated with 10 μg/mL LPS to mimic an inflammatory environment.[23]

Exosome Identification

The particle size distribution of exosomes was measured using dynamic light scattering (DLS, Malvern Instruments, Malvern, UK); The morphology was observed using transmission electron microscopy (TEM; JEOL jem-f200, Japan); Exosome-specific markers, CD9 and CD63, were determined using Western Blotting.

Synthesis and Characterization of exo@H

The hydrogels were prepared by referring to the literature.[24] PVA (Mw9000-10,000) (Sigma Chemical Co. St Louis, MO, USA) was dissolved in purified water at 95 °C from a Milli-Q system to prepare 10 mL of PVA solution containing 8% (w/v). Subsequently, 0.1 g Alg (Sigma Chemical Co. St Louis, MO, USA) was stirred and mixed with the PVA solution, and the lyophilized hucMSCs-exo was homogeneously dispersed therein and placed in a thermostatic water bath at 50 °C and stirred for 1 h at 350 r/min to form a homogeneous solution. Then, exo@H was prepared by placing calcium chloride (0.8 mL, 100 μg/mL) into the homogeneous solution under sonication and stirred to gelation it.

The surface morphology of the hydrogels and exo@H were observed by Scanning electron microscope (SEM; Hitachi Asia Ltd., Japan); After rapid quenching in liquid nitrogen, the hydrogel and exo@H were transferred to a freeze-dryer at −20 °C for 24 h and then removed. The resulting lyophilized hydrogel and exo@H samples were sprayed with gold and characterized under an accelerating voltage of 15 kV. The absorption spectra maps were determined by Fourier transform infrared spectrometer (FT-IR; Shimadzu, Kyoto, Japan), the analysis was conducted over a range of 400 to 4000 cm^{-1} at a rate of 2 cm^{-1}; The changes of energy storage mode (G') and energy dissipation mode (G'') of the hydrogel and exo@H in the range of 20–50 °C were measured by a rotating rheometer (Anton Paar MCR302), and the viscosity changes of the hydrogel and exo@H at shear rate (0–100 1/s, 37 °C) were measured by rheological analysis.

By mixing 9 μg exosomes with 300 μL of the hydrogel to obtain exo@H, and the release of exosomes was tested using the BCA Protein Analysis Kit. Briefly, the above prepared exo@H containing 9 μg of exosomes was placed in the upper permeation chamber of the Transwell while 100 μL of PBS was added to the lower chamber. 20 μL of PBS was then collected (at pH=5.5, 7.4, and 8.0 at day 0h, 2h, 4h, 6h, 8h, 10h, 12h, 24h, 2 days, 3 days, 5 days, and 7 days) and replaced by 20 μL of fresh PBS. The amount of released exosomes was detected and the percentage of exosomes release was calculated.

The hydrogel and exo@H samples were soaked in 30 mL of PBS (pH=7.4) and shaken at constant temperature. The degradation rate (Wa) of the hydrogel was calculated by weighing the initial weight of the hydrogel (W0) and the weight of the hydrogel at a predetermined time point (Wt), which were examined continuously for 7 days. The degradation equation of the hydrogel is:

$$Wa = (W0 - Wt)/W0^{*}100\% \quad (1)$$

Cell Viability Assay

MC3T3-E1 cells at a density of 5×10^3 cells/well were cultured in 96-well plate containing various concentrations of exosomes for 24 hours. The concentrations of exosomes were as follows: 1×10^7particles/mL, 1×10^8particles/mL, 1×10^9particles/mL, 1×10^{10}particles/mL. Subsequently, MC3T3-E1 cells were cultured in a-MEM complete medium containing Hydrogel, LPS, Exos, Exos+LPS, exo@H, exo@H+LPS respectively for another 24 hours, using the pure medium as the control group. Each group was replicated three times. Cell proliferation was assessed using the MTT assay, with 20 μL of MTT (5 mg/mL in PBS) added to each well and incubated at 37 °C for 4 hours. 150 μL of dimethyl sulfoxide (DMSO) was then added and incubated for 10 minutes. Finally, the optical density was analyzed at 492 nm using a microplate reader (BioTek, USA).

Alkaline Phosphatase (ALP) Staining and Quantification

MC3T3-E1 cells were seeded at a density of 1×10^5 cells/well in a 6-well plate. 24 hours later, the complete medium was replaced with osteogenic induction medium respectively containing Hydrogel, LPS, Exos, Exos+LPS, exo@H, and exo@H+LPS. After 14 days of cultivation, cells were washed in PBS, fixed for 20 minutes in a 4% paraformaldehyde neutral buffer solution, and ALP staining was conducted using a BCIP/NBT alkaline phosphatase coloration kit. ALP activity was measured using an alkaline phosphatase kit for quantitative analysis.

Alizarin Red Staining and Quantification

MC3T3-E1 cells were cultured in a 6-well plate, after 21 days of cultivation, the cells were washed three times with PBS, fixed with 95% ethanol for 10 minutes, and then stained with 0.1% alizarin red solution at 37 °C for 30 minutes. Images were captured using optical microscopy and the corresponding positive areas of alizarin red staining were measured using Image J software and determined as staining area/total area × 100%.[25]

Ligature-Induced Periodontal Model in Mice

20 seven-week-old female C57BL/6 mice were randomly allocated into four groups (N = 5): (1) Sham group, (2) Model group, (3) Hydrogel group, and (4) exo@H group. Ligation of bilateral maxillary second molars in mice under general anesthetic using 5–0 sutures.[26–28] For the sham group, sutures were immediately removed after ligation; the model group received no treatment; Starting from the second day, the hydrogel group and exo@H group were respectively treated twice daily with 50 μL of the hydrogel and 50 μL of exo@H (1.2×10^{10} particles /mL) applied around the mouse's teeth. Throughout the experiment, the ligations in all mice were kept intact. After 8 days, the mice were sacrificed using the cervical dislocation method and the maxilla was removed for further analyses.

Measurements of Bone Resorption

Maxillary alveolar bone was collected, surrounding soft tissues were removed, and stained with 0.1% methylene blue. Using the Image J software, measure the mesial and distal points on the buccal-palatal sides of the first, second, and third molars of the upper jaw of each group of mice. Measure the distance from the cement-enamel junction (CEJ) to the alveolar crest (ABC) at 12 points, take the average, to assess the alveolar bone resorption status in each mouse group.

Histological Analysis

The maxilla was immersed in 4% paraformaldehyde for 48 hours. It was decalcified in a 10% neutral Ethylene Diamine Tetraacetic Acid (EDTA) solution for 4 weeks, changing the solution every other day until a fine needle could penetrate the sample without resistance. Then it was embedded, and paraffin sections were prepared (5 μm thick), followed by hematoxylin and eosin (H&E) and tartrate-resistant acid phosphatase (TRAP) staining, and images were captured using an optical microscope. Counting of TRAP-positive multinucleated alveolar bone-associated osteoclasts at 200x magnification.

Tissue samples of the mouse's heart, liver, spleen, and kidneys were collected, routinely fixed, dehydrated, and embedded in paraffin. Subsequently, tissue sections (5 μm thickness) were made and stained with H&E to evaluate histological alterations. During the organ collection, they were weighed, and the organ index was further used to evaluate the condition of the organs in each mouse group. The organ index is calculated using:

$$\text{Organ index} = \text{weight}_{\text{organ}}/\text{weight}_{\text{body}} \times 100\% \quad (2)$$

miRNA Sequencing

Eukaryotic miRNA sequencing analysis was conducted by Seqhealth Technology Co., LTD (Wuhan, China). RNA was extracted from mouse gingival tissues using TRIzol reagent (Invitrogen, Carlsbad, CA, USA). The Small RNA Sample Pre Kit was used to construct the RNA sequencing library; based on their effective concentrations and the required downstream data volume, different libraries were pooled together and sequenced on HiseqX-10sequencer (Illumina). Next, the fastx-toolkit (version: 0.0.13.2) was utilized for data quality control; Comparative analysis of differences

between the exo@H group relative to the hydrogel group was arranged with the threshold set at an absolute FC value greater than 1.5 (|logFC|>0.585), $P < 0.05$. Finally, significantly different genes were subjected to Gene Ontology (GO) and Kyoto Encyclopedia of Genes and Genomes (KEGG) enrichment analysis.

qRT-PCR

Quantification of gene expression levels was conducted using RT-qPCR. Total RNA was extracted from mouse gingival tissues using TRIzol reagent. A stem-loop RT-PCR assay was performed to detect miRNA levels. cDNA was synthesized using PrimeScript RT Master Mix (Takara Biotechnology Co. Ltd., Dalian, China), and then amplified by SYBR® Premix Ex-Taq™ II (Takara Biotechnology Co. Ltd). Using hmGAPDH and hmU6 as internal references for mRNA and miRNA respectively, relative gene expression was calculated using the $2^{-\Delta\Delta Ct}$ method. The mRNA primer sequences for qRT-PCR are shown in Table 1. The microRNA primer sequences for qRT-PCR are shown in Table 2.

Western Blot Analysis

Proteins were lysed with RIPA buffer (Servicebio, China) containing 1% PMSF. The proteins were then quantified using the BCA protein assay kit (Servicebio, China), separated using 12% SDS-PAGE, and transferred to a PVDF membrane. The membrane was then blocked with 5% non-fat milk for 2 hours, washed three times with physiological saline containing 0.1% Tween-20 (TBST), incubated with the primary antibody at 4 °C for 12 hours, and after three more TBST washes, and then incubated with secondary antibody coupled with horseradish peroxidase (HRP) diluted 1:10,000 for 2 hours at room temperature. Immune-reactive bands were detected using enhanced chemiluminescence (ECL, Vazyme, China) and visualized with the ChemiDoc Touch Imaging System (BioRad, ChemiDoc Touch, USA). The signal intensities were measured and protein expressions were quantified using ImageJ software.

Table 1 The mRNA Primer Sequences for qRT-PCR

Primer Name	Primer Sequence (5'-3')
hmGAPDH -F	GTCAAGGCCGAGAATGGGA
hmGAPDH -R	GCAGAAGGGGCGGAGATG
Il13-4F	CCTCCCCGATACCAAAAT
Il13-4R	CTGATGTGAGAAAGGAAAATG
Nit2-2F	GCCTGGGCATCTGCTATG
Nit2-2R	AGTGGGCTGGTCCTGTGG

Table 2 The microRNA Primer Sequences for qRT-PCR

Primer Name	Primer Sequence (5'-3')
hmU6-F	CTCGCTTCGGCAGCACA
hmU6-R	AACGCTTCACGAATTTGCGT
let-7f-5p-F	CGCGCGTGAGGTAGTAGATTGT
let-7f-5p -R	AGTGCAGGGTCCGAGGTATT
miR-203-3p-F	CGCGGTGAAATGTTTAGGAC
miR-203-3p -R	AGTGCAGGGTCCGAGGTATT
let-7f-5p -RT	GTCGTATCCAGTGCAGGGTCCGAG GTATTCGCACTGGATACGACAACTAT
miR-203-3p -RT	GTCGTATCCAGTGCAGGGTCCGAGG TATTCGCACTGGATACGACCTAGTG

Luciferase Reporter Assay

Synthesize the relevant gene sequences and construct them into the pMirGLO vector. The upstream enzyme restriction site is SacI, and the downstream is XhoI. Chemically synthesize let-7f-5p and miR-203-3p. Plate logarithmic phase 293T cells in a 96-well plate and culture overnight at 37 °C with 5% CO_2 until the cell confluence reaches approximately 60%. Set up the respective experimental groups, with 3 replicate wells for each group (transfecting 300 ng of plasmid per well, with a final miRNA concentration of 50 nM). Continue culturing for 36 h after transfection. Measure the luminescence values following the procedures of the Dual-Luciferase® Reporter Assay System and analyze the results.

Statistical Analysis

All data are expressed as mean ± standard deviation (SD). Each experiment was repeated at least three times. Comparisons between two groups were performed using independent unpaired two-tailed Student's *t*-test, and comparisons between more than two groups were performed using one-way analysis of variance (ANOVA). Differences between different groups at $*P < 0.05$, $**P < 0.01$ were considered as statistically significant.

Results

Characterization of hucMSCs-exo

To determine the structural characteristics of the lyophilized hucMSCs-exo, we characterized lyophilized hucMSCs-exo by TEM, particle size distribution and Western blotting. The morphology of the exosomes is visible under the transmission electron microscope (Figure 1A), presenting as cup-disc shaped vesicles with a size of about 80 nm. As shown in the particle size distribution (Figure 1B), the diameter of the exosomes falls between 50 and 150 nm. Western blotting results (Figure 1C) demonstrate that CD9 and CD63 are highly expressed in the exosomes. These assays showed that lyophilized hucMSCs-exo conformed to the characteristics of exosomes.

Characterization of the Hydrogel and exo@H

In order to investigate the structural features of the hydrogel and exo@H, we analyzed them using scanning electron microscopy (SEM), infrared, and rheological experiments. SEM (Figure 2A and B) showed that the hydrogel and exo@H have a three-dimensional mesh structure. FT-IR (Figure 2C) can observe that there is no difference in the wavelengths of the groups between the hydrogel and exo@H. As shown in Figure 2D, the G' of the hydrogel and exo@H was always larger than G'' under different temperature conditions; indicating that the two hydrogels have good viscosity and stability. Figure 2E shows the change in viscosity at variable shear rates, where the viscosity of the gel decreases significantly when the shear rate is increased immediately, and decreases slowly and tends to change slightly when the gradual increase in shear rate is applied, showing a behavior consistent with shear thinning. Figure 2F shows the release properties of the hydrogel loaded exosomes. The exosomes showed a gradual release trend with time, and a controlled, smooth and sustained release was satisfied under different pH conditions. Figure 2G shows the degradability of the hydrogel, our prepared exo@H showed a gradual degradation trend with time, and the continuous degradation could be maintained within 7 days. These results indicate that the exo@H delivery system we constructed has good structural stability and some viscoelasticity and can be used in a mouse model of periodontitis.

Exo@H Promotes the Proliferation and Osteogenic Differentiation of MC3T3-E1 Cells

To detect the effect of different concentrations of exosomes on the proliferation of MC3T3-E1 cells, MTT experiments were performed. As shown in Figure 3A, the highest efficiency was observed at the concentration of 1×10^9particles/mL. To investigate whether exo@H could induce MC3T3-E1 cells proliferation, we further examined the cell viability of MC3T3-E1 cells under various conditions including Control, Hydrogel, LPS, Exos, Exos+LPS, exo@H, and exo@H +LPS. By mimicking a periodontal inflammation environment with LPS, we observed that LPS substantially suppressed cells growth when compared to the control. The hydrogel did not influence MC3T3-E1 cells proliferation, but exosomes did amplify it. Furthermore, the exo@H group demonstrated a higher proliferation rate than the exosomes group.

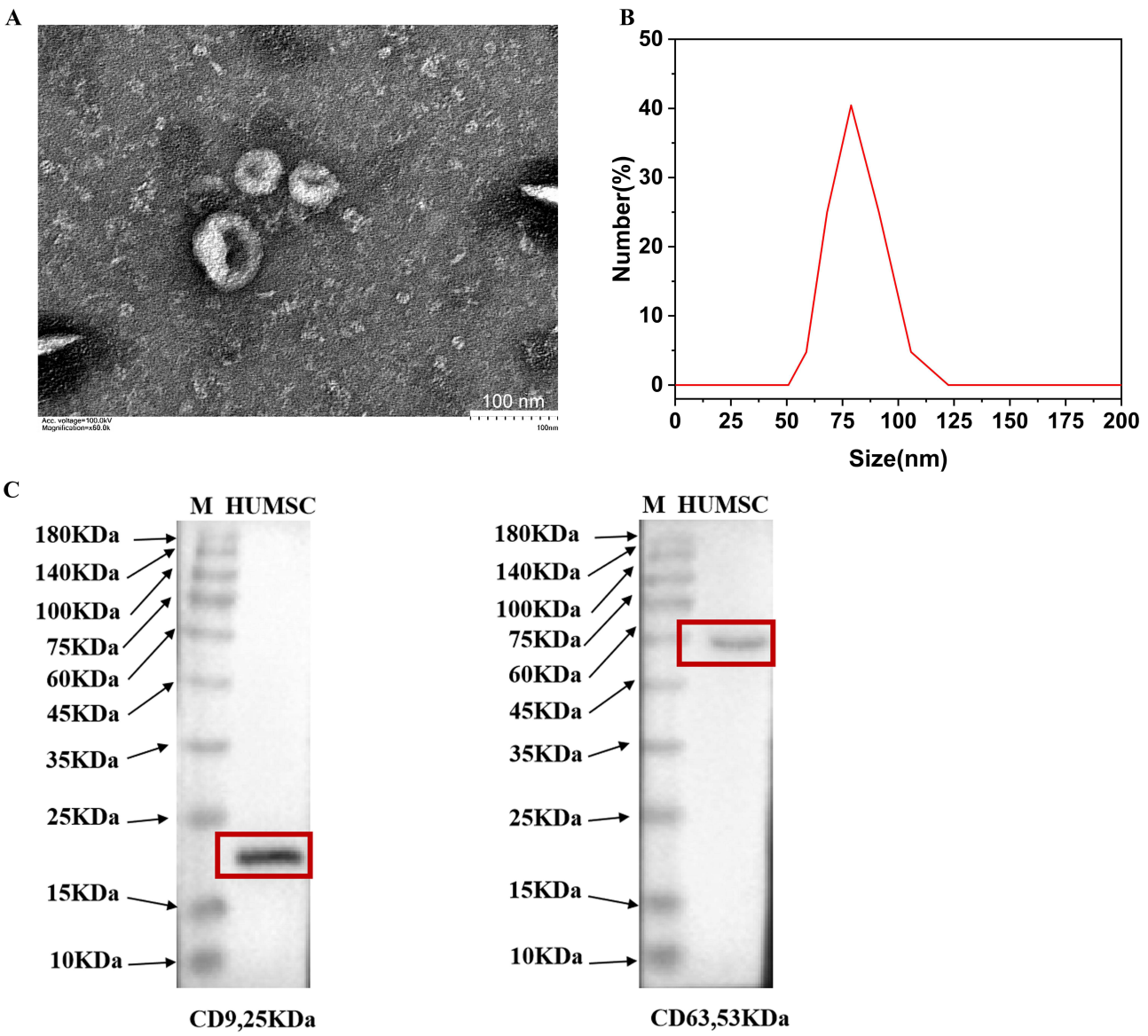

Figure 1 Characterization of lyophilized hucMSCs-exo. (**A**) TEM observation of exosome morphological characteristics (Scale bar: 100 nm). (**B**) NTA detection of exosome particle size distribution. (**C**) Western Blot detection of exosome markers.

The effect of exo@H on osteogenic differentiation of MC3T3-E1 cells was observed by ALP assay. After 14 days of osteogenic induction, the results of the ALP quantification assay (as shown in Figure 3D) revealed that the inflammation group treated with LPS displayed lower ALP activity compared to the non-inflammation group without LPS treatment, exo@H significantly enhanced the ALP activity of MC3T3-E1 cells. ALP staining results were consistent with the results of quantitative experiments (Figure 3B).

The effect of exo@H on osteogenic differentiation of MC3T3-E1 cells was observed by alizarin red assay. After 21 days of osteogenic induction, alizarin Red staining and quantification assay (Figure 3C and E) illustrated distinct variations in osteogenic differentiation of MC3T3-E1 cells subjected to different treatments. LPS markedly suppressed the differentiation into osteoblasts, whereas exo@H greatly enhanced this differentiation process.

Exo@H Reduces Alveolar Bone Resorption in Periodontitis Mice

To assess the impact of exo@H on mice with periodontitis, we established an animal model of periodontitis using the ligation method (Figure 4A and F). The maxillary bones of the experimental mice were collected and analyzed using

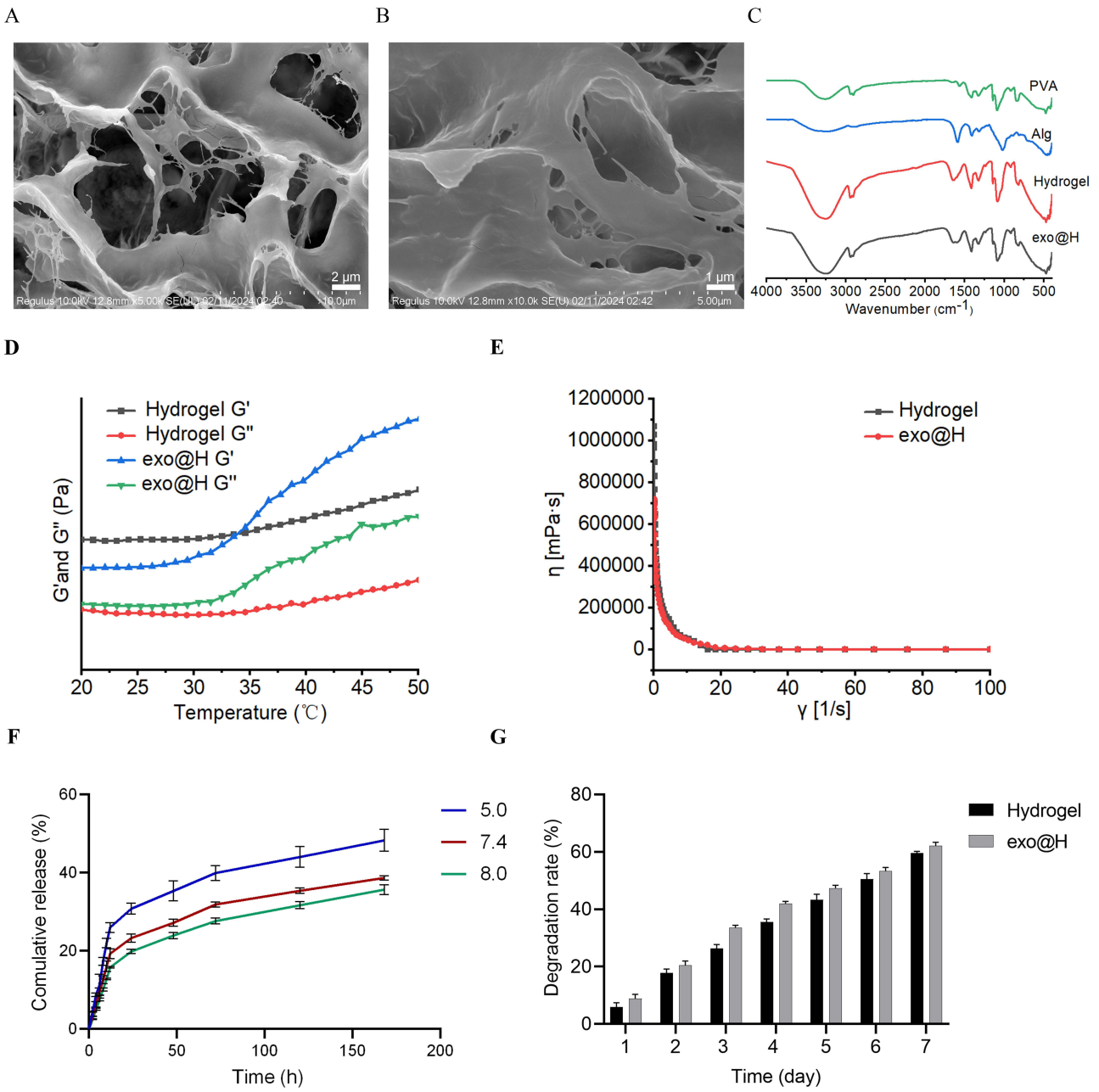

Figure 2 Material characterization. (**A**) SEM images of hydrogel (Scale bar: 10 μm). (**B**) SEM images of exo@H (Scale bar: 5 μm). (**C**) FT-IR analysis of PVA, Alg, hydrogel and exo@H. (**D**) The hydrogel and exo@H energy storage modes, variation of energy dissipation modes with temperature. (**E**) Variation of hydrogel and exo@H fluidity with shear stress. (**F**) Release profiles of the hydrogel loaded exosomes. (**G**) Degradation rates of the hydrogel and exo@H.

a stereomicroscope and bone measurement (Figure 4B-E). The results showed that the ABC-CEJ distance in the model group was significantly greater than in the sham group. The hydrogel had no effect on alveolar bone absorption, whereas the ABC-CEJ distance in mice treated with exo@H was noticeably reduced. It indicated that exo@H was able to inhibit bone resorption in periodontitis mice.

We used H&E staining to observe the changes in the periodontal tissues, and H&E staining reveals (Figure 5A and C) increased CEJ-ABC distance in the model group, significant destruction of the alveolar bone, with a substantial infiltration of inflammatory cells observed in the surrounding connective tissue. There were no significant differences observed between the hydrogel group and the model group. In the exo@H group, both bone destruction and inflammatory responses were reduced.

https://doi.org/10.2147/IJN.S502192

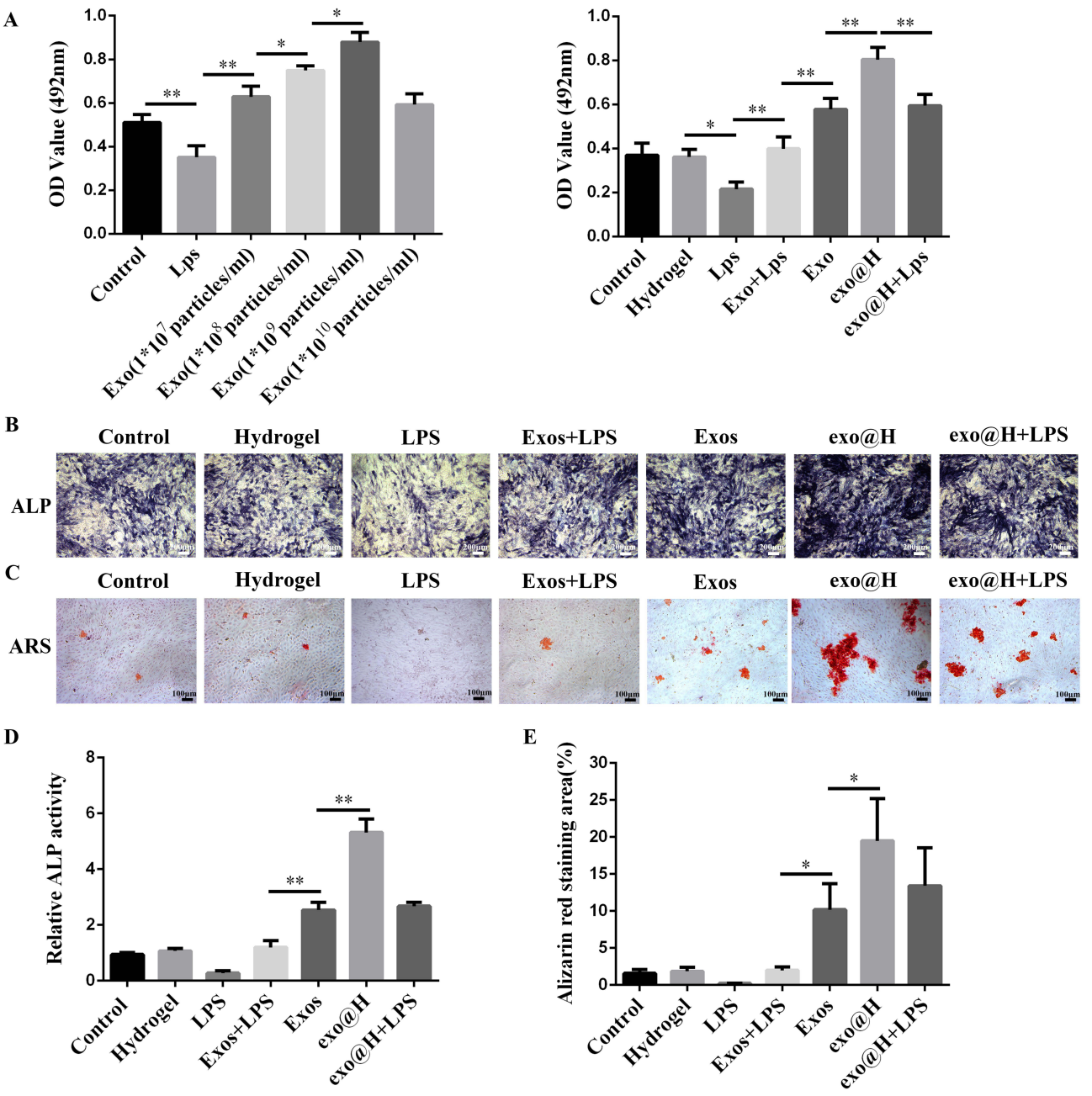

Figure 3 Influence of exo@H on the proliferation and osteogenic differentiation of MC3T3-E1 cells. (**A**) MC3T3-E1 cells proliferation assay by MTT; **P*<0.05, ***P*<0.01. (**B**) ALP staining (Scale bar: 200 μm). (**C**) Alizarin Red S staining (Scale bar: 100 μm). (**D**) ALP activity quantification assay; ***P*<0.01. (**E**) Quantitative analysis of the corresponding positive area of alizarin red staining; **P* <0.05.

We used TRAP staining to observe the expression of osteoclasts in periodontal tissues, and TRAP staining is shown in (Figure 5B), compared to the sham group, the model group displayed a dense distribution of osteoclasts along the alveolar bone margins. The periodontal tissues of mice treated with the hydrogel for periodontitis also exhibited a high number of osteoclasts. Conversely, a noticeable reduction in osteoclasts was observed in the periodontal tissues of periodontitis mice treated with exo@H.

The Effect of exo@H on Organ Slices and Organ Index

H&E staining of organ sections (Figure 6A) indicated that the organ structures in experimental mice were normal, with no apparent organ damage. The organ index results (Figure 6B) showed that there were no statistically significant

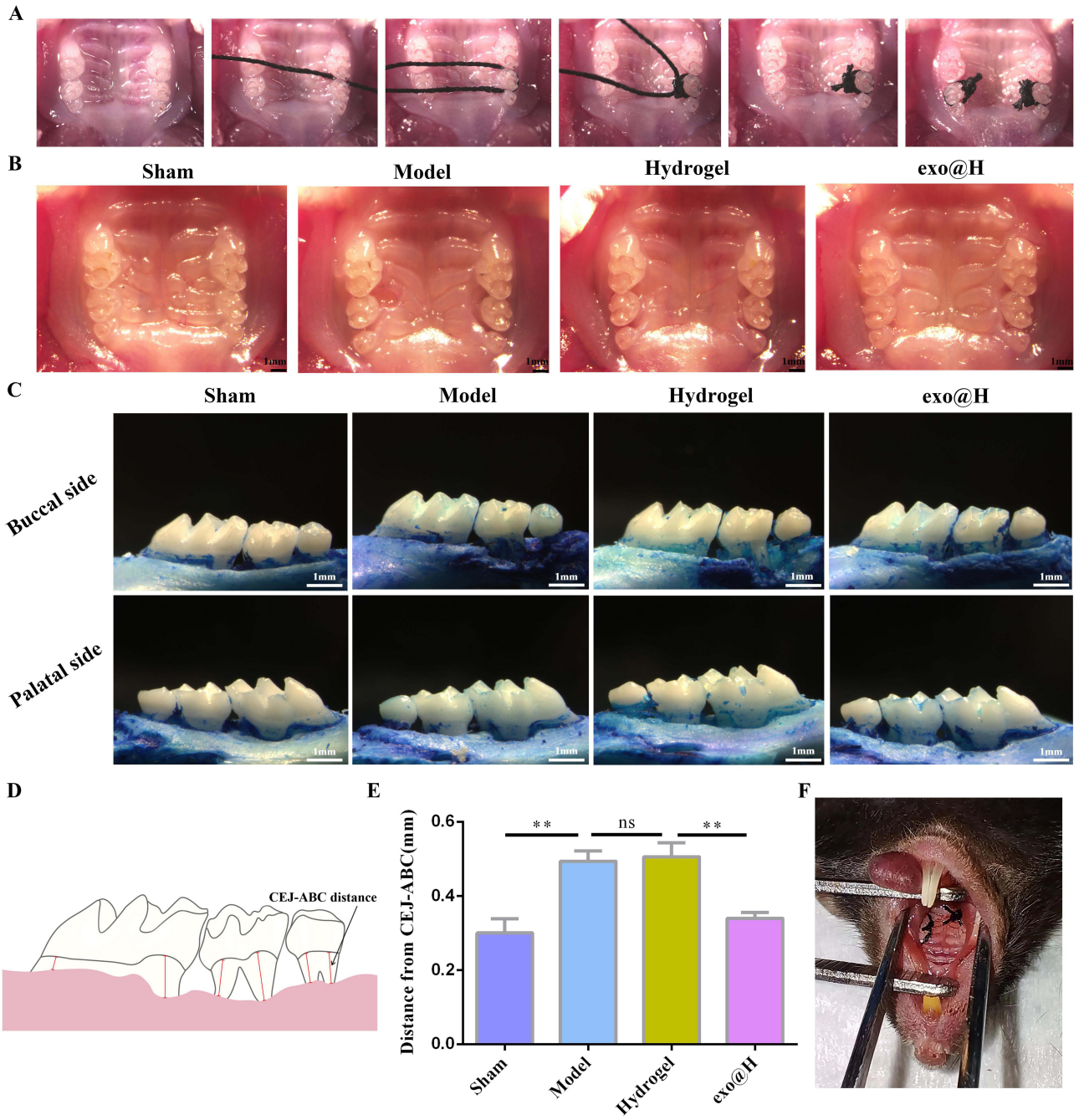

Figure 4 Exo@H alleviates alveolar bone absorption in mice with periodontitis. (**A**) Technical procedure of the ligation model. (**B**) Representative images of maxillary periodontal tissues in mice; scale bar is 1 mm. (**C**) Effectiveness of periodontitis treatment in different experimental groups; scale bar is 1 mm. (**D**) Schematic diagram of bone resorption measurement methods. (**E**) Quantification of ABC-CEJ distance in maxillary molars; $^{**}P<0.01$. (**F**) Periodontitis model.

differences in the indices for the heart, liver, spleen, and kidneys ($P > 0.05$). It indicates that exo@H is safe and non-toxic.

Analysis of the Differential Expression of miRNAs

To study the therapeutic mechanism of exo@H on periodontitis in mice, we performed RNA sequencing analysis on the gingival tissues of the experimental mice. We previously found that there was no significant difference between the model group and the hydrogel group. The results showed that (Figure 7A and B), compared to the hydrogel group, in the exo@H group, 59 miRNAs were upregulated and 92 miRNAs were downregulated, and the results were illustrated using

https://doi.org/10.2147/IJN.S502192

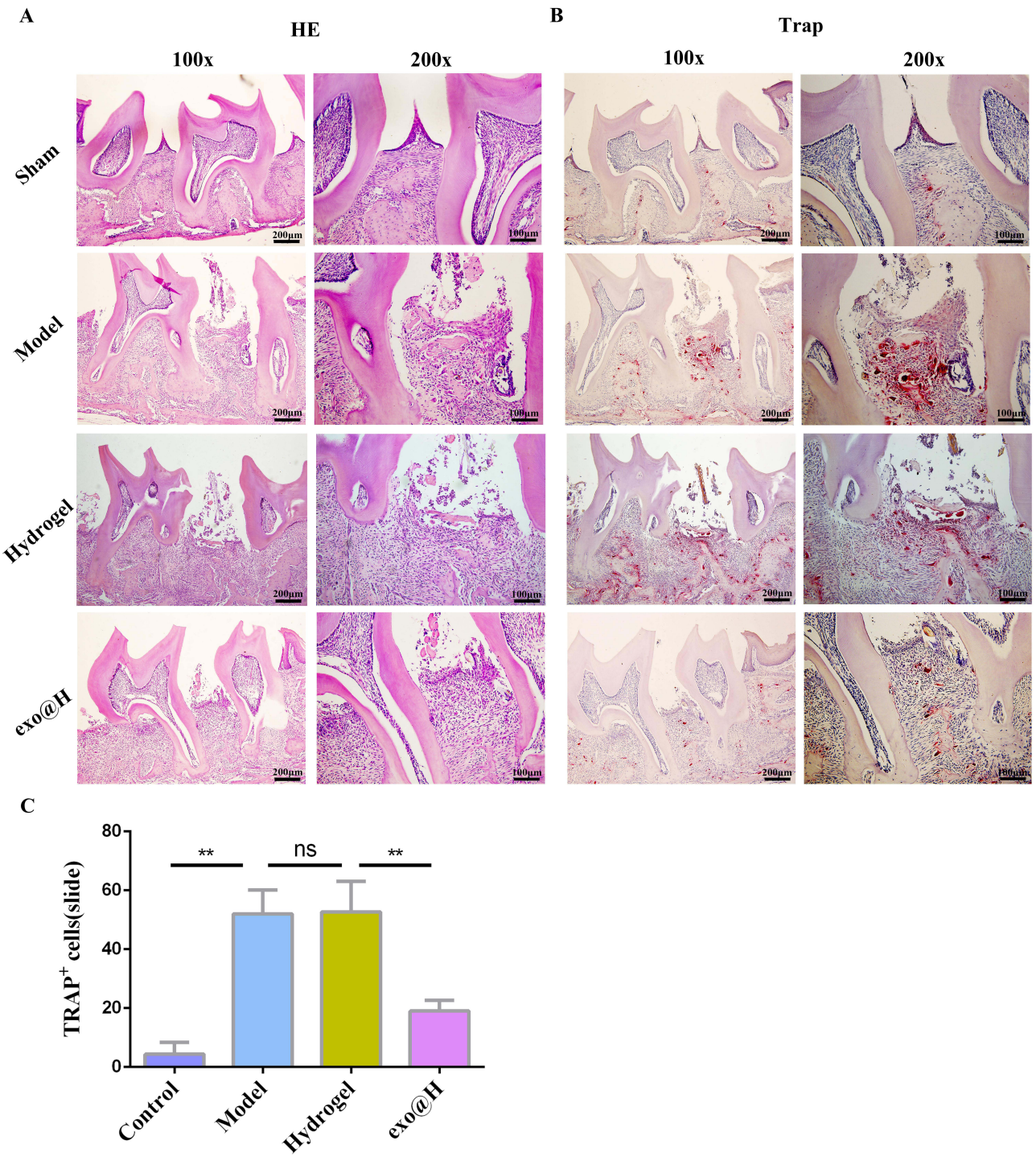

Figure 5 Histological observation of periodontal tissue. (**A**) H&E staining. (**B**) TRAP staining. (**C**) TRAP staining positive osteoclast count; ***P*<0.01.

a heat map (Figure 7F). The Venn diagram (Figure 7C) shows that compared to the hydrogel group, the exo@H group has 673 genes upregulated and 4349 genes downregulated, with 424 genes overlapping between the two groups. Among both groups, 10 miRNAs showed significant expression along with their related target genes, including the upregulated let-7f-5p with IL-13, let-7c-5p with Pld3 and Masp1, miR-125b-5p with Rac3, miR-203-3p with Nit2, miR-16-5p with Pnp2, and let-7a-5p with IL-13 and Pld3, as well as the downregulated miR-34c-5p with Dll1, miR-214-3p with Dll1,

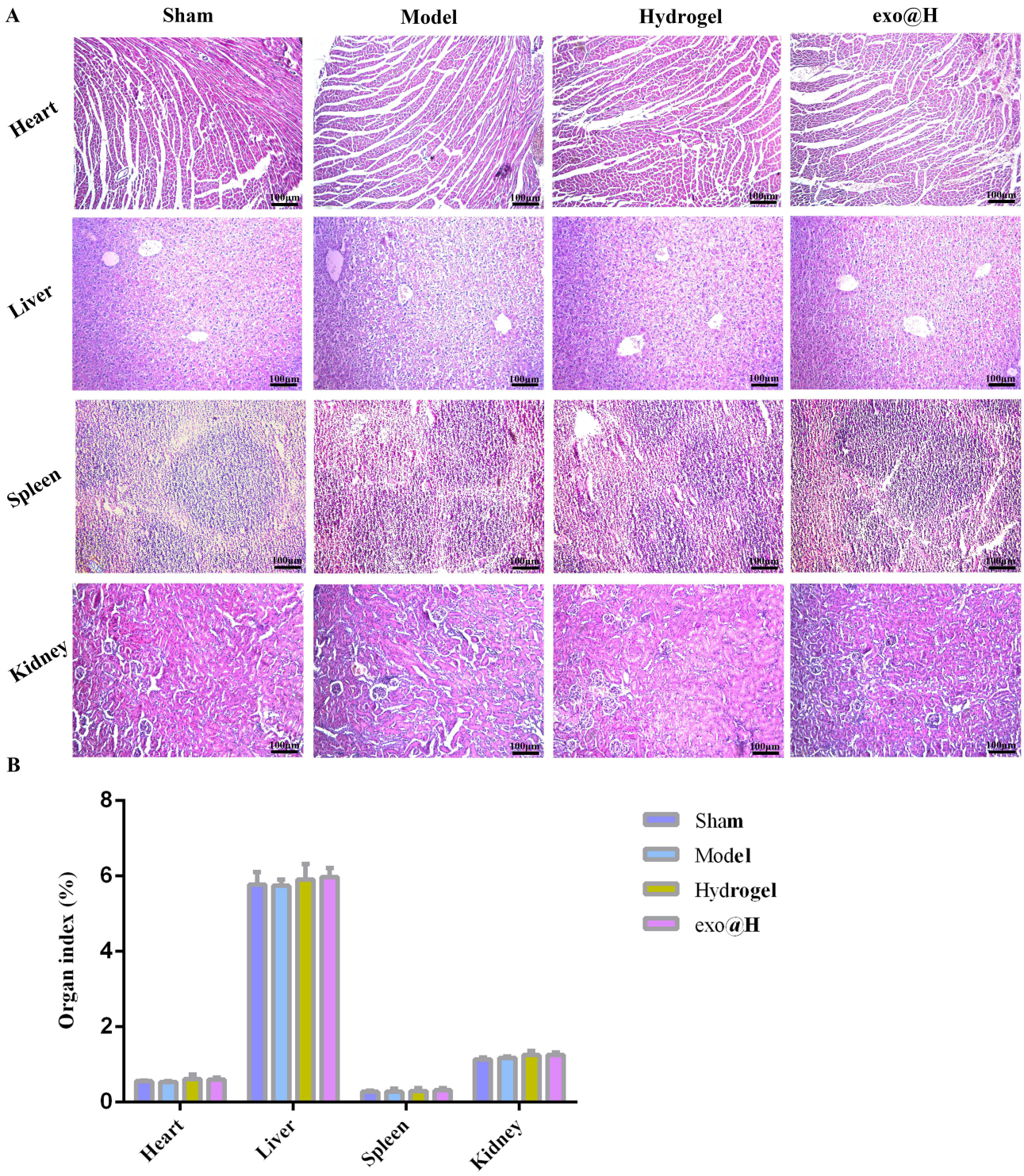

Figure 6 Impact of exo@H on organ sections and organ indices. (**A**) Histological examination of mouse heart, liver, spleen, and kidney sections. (**B**) Organ indices.

Rac2, and Pld2, miR-1198-5p with Hras and Hdac2, and miR-320-3p with Gng8. In addition, genes shared between multiple groups were shown by performing Venn analysis on different groups (Figure 7D and E).

GO Functional Analysis and KEGG Pathway Analysis

Next, we conducted GO enrichment analysis and KEGG database analysis on the 10 significantly expressed miRNAs, and found (Figure 8) that the 6 upregulated miRNAs primarily influence metabolic pathways, the complement system, and the

https://doi.org/10.2147/IJN.S502192

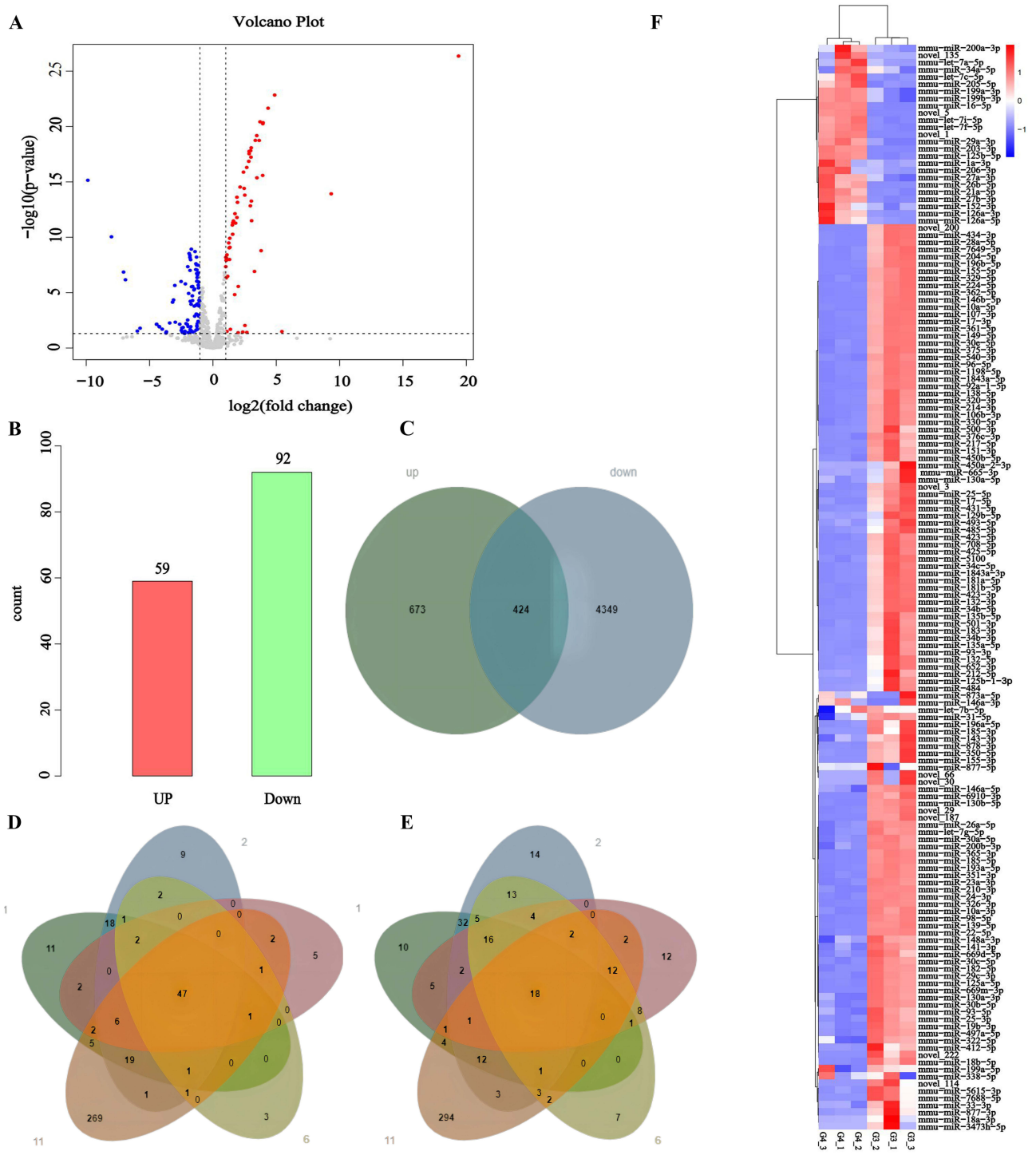

Figure 7 Differential miRNA expression between exo@H group and hydrogel group. (**A**) Volcano plot of differentially expressed miRNAs. (X-axis log2(fold change): Logarithm to the base 2 of the fold change; Y-axis -log10(*p*-value): Negative logarithm to the base 10 of the *p*-value; Gray dots represent miRNAs with no differential expression, blue dots represent downregulated miRNAs, and red dots represent upregulated miRNAs. (**B**) Count of differentially expressed miRNAs showing upregulation and downregulation. (**C**) Venn diagram of target genes between the exo@H group and the hydrogel group. (**D**) Venn analysis of upregulated genes among the groups. (**E**) Venn analysis of downregulated genes among the groups. (1 represents model group/sham group; 2 represents Hydrogel group/sham group; 5 represents exo@H group/model group; 6 represents exo@H group/hydrogel group; 11 represents exosomes.) (**F**) Heatmap indicates differentially expressed miRNAs between the two groups. (G3 represents the hydrogel group, G4 represents the exo@H group.).

differentiation of Th1 and Th2 cells, whereas the 4 downregulated miRNAs predominantly modulate inflammatory responses through several pathways, including the Notch signaling pathway, Ras signaling pathway, MAPK signaling pathway, and the Fc epsilon RI signaling pathway, suggesting their potential as therapeutic targets for periodontitis.

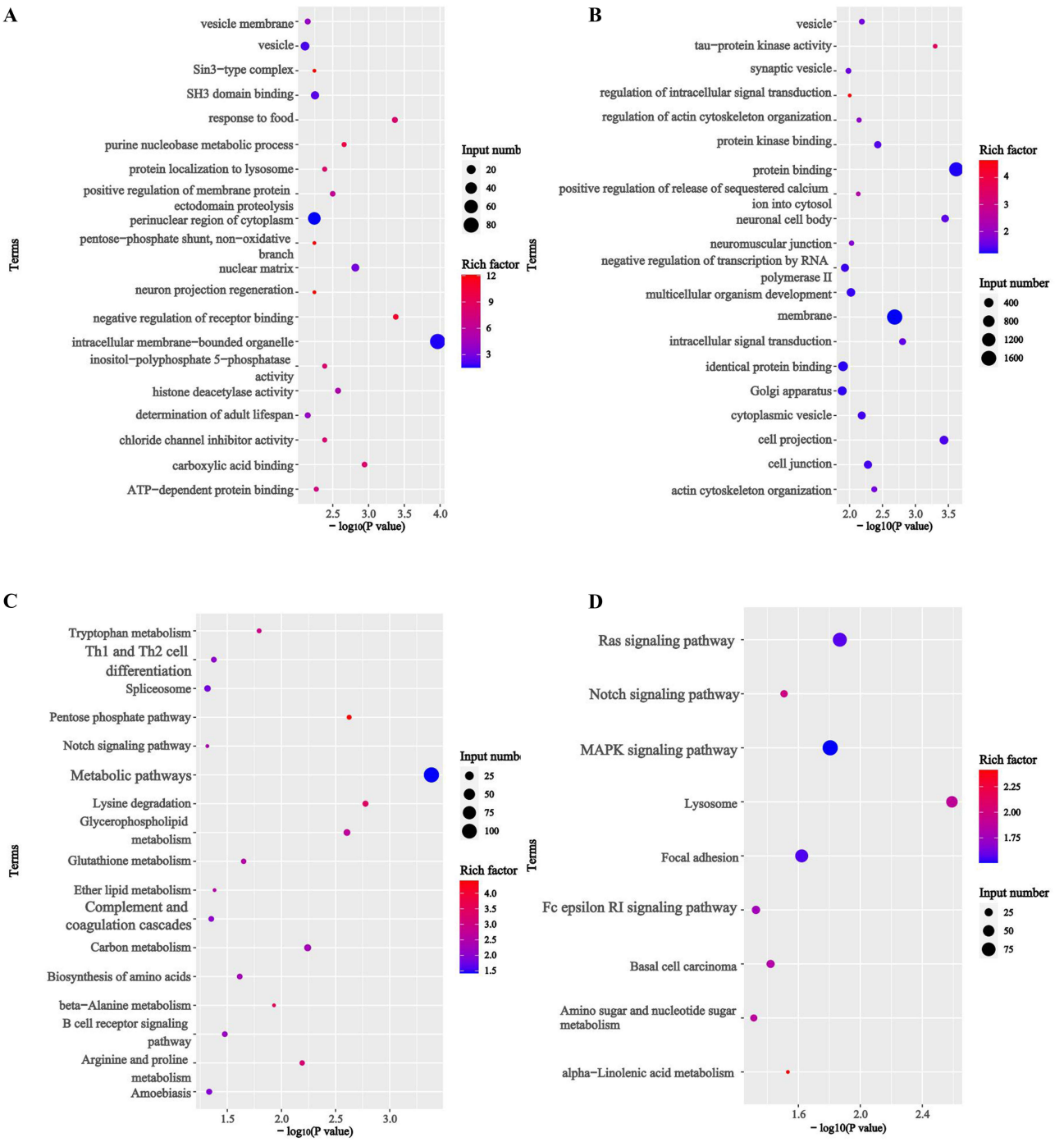

Figure 8 GO and KEGG enrichment analysis of differentially expressed miRNAs. (**A**) GO enrichment of up-regulation expressed miRNAs. (**B**) GO enrichment of down-regulation expressed miRNAs. (**C**) KEGG pathway analysis identifying upregulated differentially expressed genes. (**D**) KEGG pathway analysis identifying downregulated differentially expressed genes.

Validation of Differentially Expressed miRNAs

Among the differentially expressed miRNAs, we selected let-7f-5p and miR-203-3p, which expressed significantly, for further study, and their predicted related target genes were tested. The RT-PCR results showed (Figure 9A) that compared to the periodontitis mice treated with the hydrogel, the levels of let-7f-5p and miR-203-3p in the gingival tissues of periodontitis mice treated with exo@H were significantly elevated, while the levels of IL-13 and Nit2 in the periodontal tissues also significantly increased.

https://doi.org/10.2147/IJN.S502192

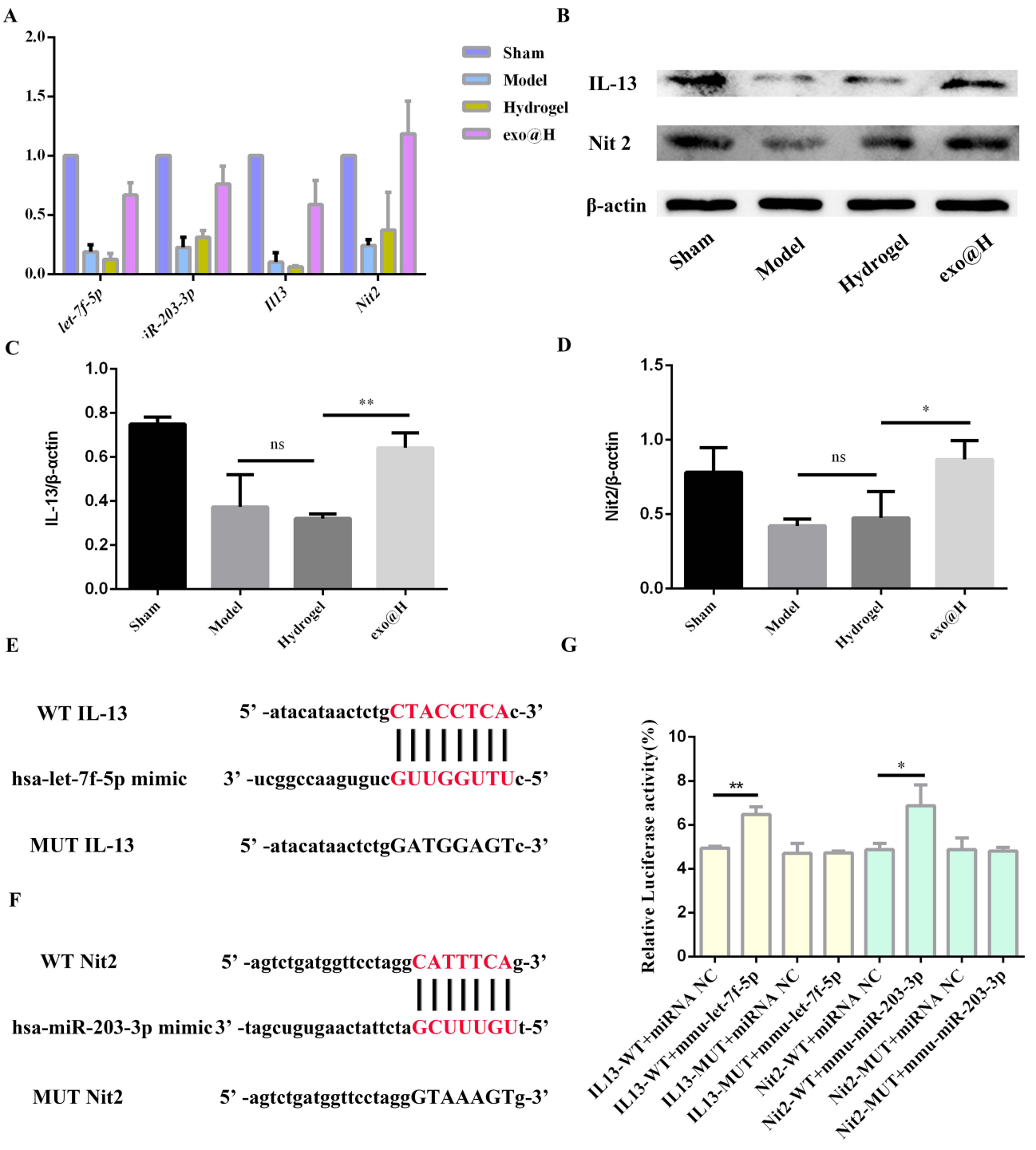

Figure 9 Luciferase reporter assays validate miRNA targets. (**A**) miRNA-qPCR to detect the expression levels of let-7f-5p with IL-13 and miR-203-3p with Nit2. (**B**) Western blotting to assess the protein expression levels of IL-13 and Nit2. (**C**) Quantitative analysis of IL-13 expression levels by Western blot, data represents mean ± standard deviation (n=3), **P*<0.05, ***P*<0.01. (**D**) Quantitative analysis of Nit2 expression levels by Western blot, data represents mean ± standard deviation (n=3), **P*<0.05, ***P*<0.01. (**E**) The predicted binding site between the let-7f-5p and IL-13. (**F**) The predicted binding site between the miR-203-3p and Nit2. (**G**) Relative luciferase activity; **P*<0.05, ***P*<0.01.

Western blotting analysis further confirmed that compared to the hydrogel group, the expression of Nit2 and IL-13 in the exo@H treatment group was upregulated (Figure 9B–D). The trends in protein levels and RNA expression were consistent, further validating the role of exo@H in periodontal tissues.

Let-7f-5p Targets to IL-13, miR-203-3p Targets to Nit2

Luciferase reporter assays were performed to confirm the direct binding relationship between IL-13 and let-7f-5p (Figure 9E and G). The results showed that let-7f-5p may target the 3'UTR of IL-13, and the CTACCTCA site may be the binding site where let-7f-5p targets IL-13. Luciferase reporter assays were performed to confirm the direct binding relationship between Nit2 and miR-203-3p (Figure 9F and G). Results indicated that miR-203-3p might target the 3'UTR of Nit2, and the CATTTCA site could be the binding location where miR-203-3p targets Nit2.

Discussion

Periodontitis is one of the most common chronic diseases known to humans, with as many as 24% of the global population affected by severe periodontal disease, affecting more than 1 billion people.[29] However, achieving effective treatment for periodontitis remains challenging. In this study, our results suggested that exo@H alleviated experimental periodontitis in mice partly by delivering miRNAs which regulated gene expression in periodontal tissues.

In recent years, MSCs have been widely used as cell therapies for a variety of diseases based on their unique abilities of self-renewal, multidirectional differentiation and immunomodulation.[30] In addition, studies have shown that MSCs can be successfully used in the treatment of periodontitis.[31] Considering the ethical regulatory constraints and the time and cost of preparing large quantities of cells, we chose hucMSCs, which are generated from umbilical cords, and which not only have triple efficacy in terms of tissue repair, immunomodulation and anticancer properties, but can also be obtained at low cost without ethical issues and produce little or no immune rejection in vivo.[32,33] Reports suggest that MSCs therapy achieves its therapeutic effects mainly through the release of secretome-derived bioactive factors, particularly exosomes.[34,35] A previous study by our group found that hucMSCs-exo could accelerate diabetic wound healing by promoting angiogenesis.[22] Based on the unique advantages of hucMSCs-exo and the foundation of its prior application to the skin, we used it for the treatment of experimental periodontitis in mice. We speculate that hucMSCs-exo may be ideal for clinical use in periodontitis treatment.

Exosomes, as a promising cell-free therapeutic approach, face challenges in terms of long-term storage. It has been reported that freeze-drying does not disrupt the structural integrity and biological activity of exosomes, nor does it compromise the stability of their protein and lipid components. Moreover, lyophilized exosomes facilitate sample transportation, reduce storage and transportation costs, and address biosecurity concerns by preventing sample cross-contamination.[36–38] However, the effect of lyophilized exosomes on periodontitis remains unclear. In our study, we characterized the lyophilized hucMSCs-exo by three different methods, TEM, NTA and Western Blot, which showed that the lyophilized hucMSCs-exo was within the acceptable quality range in terms of morphology, size and enrichment of protein markers, further suggesting that lyophilization was an ideal solution to the challenge of long-term storage of exosomes. To improve exosome delivery and overcome the current limitations, we prepared a hydrogel in which -OH enhances hydrophilicity and forms hydrogen bonds with water molecules to increase the viscosity and strength of the hydrogel,[39] and -COO- promotes the transformation of the hydrogel by cross-linking to control drug release. In addition, -COO- and -OH form a dynamic non-covalent bonding scaffold, which endows the hydrogel with good self-healing ability and shear-thinning properties.[40]

We constructed a drug delivery system of hydrogel-loaded lyophilized hucMSCs-exo for the treatment of periodontitis. G' is always greater than G'' at 35–40 °C, indicating that it is always in the gel state, exo@H can provide a stable drug delivery system in the dynamic biological environment of the human body (37 °C). The variable shear stress, furthermore, can modulate the hydrogel viscosity so that it acts at a specific site, which has important implications for translation into practical biomedical applications. Under the physiological conditions of pH in the oral cavity, exosomes are stabilized and slowly released from the hydrogel to achieve good therapeutic effects, and the hydrogel and exo@H are slowly degraded in vivo over time, with the degradation rate following the trend of exosome release. In vitro, lyophilized hucMSCs-exo enhanced the cell proliferation and calcium deposition capacity during osteogenic induction, and exo@H better enhanced the effect of lyophilized hucMSCs-exo on promoting osteogenic induction, suggesting that combining with hydrogels better exerts the efficacy of exosomes. Using ligation-induced periodontitis mice, exo@H effectively alleviated periodontal inflammation and inhibited bone resorption in periodontitis mice, indicating that exo@H exerts a protective effect against

periodontitis. Furthermore, no signs of cytotoxicity were observed in heart, liver, spleen, and kidney tissues, and mice treated with exo@H exhibited no signs of discomfort, suggesting that exo@H is safe for use.

Exosomes are extracellular vesicles rich in a variety of substances such as proteins, lipids and nucleic acids. It was found that hucMSCs-exo was enriched in various miRNAs and that hucMSCs-exo regulates inflammatory responses and promotes tissue healing mainly through miRNAs.[41,42] MiRNAs, as a crucial part of regulating gene expression, is a highly complex process, which mainly regulates gene expression post-transcriptionally, and changes in miRNA levels are highly sensitive and specific.[43,44] Once an imbalance occurs and an abnormal miRNA is present, it can lead to disease. It has been shown that miRNAs can participate in osteogenic differentiation by regulating runt-related transcription factor 2 (RUNX2) and osteoprotegerin (OPG), osteoclastogenesis by regulating nuclear factor-kB ligand receptor activator (RANKL), and inflammatory factors such as interleukin-6 (IL-6), IL-1 and tumor necrosis factor-alpha (TNF-α) inflammatory response. At the same time, the inflammatory response also promotes osteoclast differentiation and osteoblast inhibition. This may be related to the involvement of exosomes in the OPG-RANKL-RANK signaling pathway to regulate osteoclast function and influence the inflammatory immune response, thereby inhibiting bone resorption and inflammatory damage of periodontal tissues in periodontitis.[45]

The involvement of miRNAs in periodontal homeostasis has been much reported previously. Adomas Rovas et al used microarray technology to analyze inflammatory gingival miRNA expression in patients with chronic periodontitis and found that 30 miRNAs were upregulated and 23 miRNAs were downregulated.[46] K J Nisha et al found that 40 miRNAs were highly expressed and 40 were lowly expressed in the saliva of patients with chronic periodontitis using high pass sequencing technique.[47] The inconsistency between the findings of the two groups of researchers suggests that the development of periodontitis is a dynamic and variable process, and the miRNAs involved in regulation may be different at different stages of development. In our study, we found that compared with the hydrogel group, the exo@H group had 59 miRNAs up-regulated such as let-7f-5p, let-7c-5p, miR-125b-5p, miR-203-3p, miR-16-5p, let-7a-5p, and 92 miRNAs down-regulated such as miR-34c-5p, miR-214-3p, miR-1198-5p, miR-320-3p, and 92 miRNAs were down-regulated, which may be involved in the maintenance of periodontal homeostasis by affecting metabolic pathways and cell differentiation, and may control inflammatory responses, inhibit osteoclast activity and promote osteoblast differentiation by modulating Notch signaling pathway, Ras signaling pathway, and MAPK signaling pathway. This suggests that hucMSCs-exo can reduce the degree of inflammation and promote tissue repair in diseased periodontal tissues through differentially expressed miRNAs.

Previous studies have focused on analyzing differentially expressed miRNAs and identifying their associated target genes in different periodontal microenvironments, neglecting the interaction network constituted between multiple miRNAs, which is also a major drawback of our study. The validation of single miRNAs and their corresponding target genes is partial and cannot fully reflect the mechanism of action of using miRNAs to treat periodontitis. In the present study, we chose let-7f-5p and miR-203-3p, which are significantly differentially expressed, for further study, aiming to provide more comprehensive support for the treatment of periodontitis using miRNAs. The let-7 family is the earliest known miRNA identified in humans and is highly conserved across species in terms of sequence and function.[48] Let-7f-5p was found to promote vascularization and bone formation.[49,50] MiR-203, located on chromosome 14q32.33,[51] and is involved in tissue development, homeostasis and maintenance of function, alleviation of inflammatory responses and promote bone formation.[52,53] In this study, we confirmed the positive regulation of let-7f-5p and miR-203-3p with their predicted target genes IL-13 and Nit2, and we found that exo@H up-regulated the expression of let-7f-5p and miR-203-3p as well as their corresponding target genes IL-13 and Nit2 in the periodontal tissues of mice. IL-13 has been reported to have anti-inflammatory effect and inhibit a range of TNF-α-induced diseases, such as collagenous arthritis, LPS-induced inflammatory diseases, and acute lung injury.[54] Nit2 is commonly expressed in tissues and encodes proteins that is predominantly distributed in the cytoplasm and is involved in cell growth and homeostatic maintenance through nitrogen-sulfur metabolism.[55,56] In this study, we concluded that hucMSCs-exo is involved in cell metabolism and cell differentiation through the upregulation of let-7f-5p and miR-203-3p, which regulate multiple inflammatory pathways, thereby promoting the expression of the anti-inflammatory factor IL-13 and the metabolic factor Nit2, which are involved in inflammatory control and tissue repair in periodontitis.

Using miRNAs to regulate gene expression for the treatment of periodontitis is still in the preliminary stage of exploration, and in-depth studies are needed to investigate the mechanism and function of miRNAs targeting genes in the

periodontal microenvironment. In addition, the antimicrobial properties of hucMSCs-exo, the long-term effects on systemic health, and the assessment of biomarkers of systemic toxicity are still unknown and need to be further explored in future studies. Based on the therapeutic potential of exosomal miRNAs, it provides a promising research direction for disease diagnosis and treatment. However, questions such as the selection and combination of different target genes for miRNAs in the treatment of periodontal disease, the mutual interactions among multiple miRNAs, and the control of their dosage during application all require further investigation.

Existing reports on the application of exosomes are mostly administered by injection,[57,58] and administrating multiple injections exacerbates the irritation of tissues, and brings bad experiences and pain to the patient. Here we tried a simple and conducive to the acceptance of the patient's periodontal coated administration. This approach facilitates the gradual penetration of drugs into the periodontal tissues, enhancing therapeutic efficacy, and is straightforward and practical, making it more suitable for future clinical translation.

Conclusion

In this study, we successfully constructed a hydrogel-loaded lyophilized hucMSCs-exo drug delivery system. We found that exo@H promoted the proliferation and calcification of MC3T3-E1 cells and supported bone regeneration and repair. By delivering miRNAs, such as let-7f-5p and miR-203-3p, which positively regulate IL-13 and Nit2, respectively, it attenuates the inflammatory response of periodontal tissues and promotes tissue repair. Our study provides a new idea for periodontitis treatment. In addition, screening characteristic miRNAs and analyzing the regulatory mechanisms of their target genes may provide new clues for targeted therapy of periodontitis.

Data Sharing Statement

Data will be made available on request.

Acknowledgments

This work was supported by the National Natural Science Foundation of China (Grant no. 81600870), and by grant from General Project Supported by Natural Science Foundation of Liaoning Province (2021-MS-324).

Disclosure

The authors declare that they have no known competing financial interests or personal relationships that could have appeared to influence the work reported in this paper.

References

1. Hajishengallis G, Chavakis T. Local and systemic mechanisms linking periodontal disease and inflammatory comorbidities. *Nat Rev Immunol*. 2021;21(7):426–440. doi:10.1038/s41577-020-00488-6
2. Rinčić G, Gaćina P, Virović Jukić L, Rinčić N, Božić D, Badovinac A. ASSOCIATION BETWEEN PERIODONTITIS AND LIVER DISEASE. *Acta Clin Croat*. 2022;60(3):510–518. doi:10.20471/acc.2021.60.03.22
3. Qiao X, Tang J, Dou L, et al. Dental pulp stem cell-derived exosomes regulate anti-inflammatory and osteogenesis in periodontal ligament stem cells and promote the repair of experimental periodontitis in rats. *Int J Nanomed*. 2023;18:4683–4703. doi:10.2147/ijn.S420967
4. Shen Y, Cai J. The importance of using exosome-loaded miRNA for the treatment of spinal cord injury. *mol Neurobiol*. 2023;60(2):447–459. doi:10.1007/s12035-022-03088-8
5. Yin K, Wang S, Zhao RC. Exosomes from mesenchymal stem/stromal cells: a new therapeutic paradigm. *Biomark Res*. 2019;7(1):8. doi:10.1186/s40364-019-0159-x
6. Lu Y, Huangfu S, Ma C, et al. Exosomes derived from umbilical cord mesenchymal stem cells promote healing of complex perianal fistulas in rats. *Stem Cell Res Ther*. 2024;15(1):414. doi:10.1186/s13287-024-04028-0
7. Teng L, Maqsood M, Zhu M, et al. Exosomes derived from human umbilical cord mesenchymal stem cells accelerate diabetic wound healing via promoting m2 macrophage polarization, angiogenesis, and collagen deposition. *Int J mol Sci*. 2022;23(18):10421. doi:10.3390/ijms231810421
8. Hu Z, Jiang Z, Meng S, Liu R, Yang K. Research progress on the osteogenesis-related regulatory mechanisms of human umbilical cord mesenchymal stem cells. *Stem Cell Rev Rep*. 2023;19(5):1252–1267. doi:10.1007/s12015-023-10521-5
9. Gao S, Dong Y, Yan C, Yu T, Cao H. The role of exosomes and exosomal microRNA in diabetic cardiomyopathy. *Front Endocrinol*. 2023;14:1327495. doi:10.3389/fendo.2023.1327495
10. Zabalza A, Pappolla A, Comabella M, Montalban X, Malhotra S. MiRNA-based therapeutic potential in multiple sclerosis. *Front Immunol*. 2024;15:1441733. doi:10.3389/fimmu.2024.1441733

11. Peng L, Chen Y, Shi S, Wen H. Stem cell-derived and circulating exosomal microRNAs as new potential tools for diabetic nephropathy management. *Stem Cell Res Ther*. 2022;13(1):25. doi:10.1186/s13287-021-02696-w
12. Nakao Y, Fukuda T, Zhang Q, et al. Exosomes from TNF-α-treated human gingiva-derived MSCs enhance M2 macrophage polarization and inhibit periodontal bone loss. *Acta Biomater*. 2021;122:306–324. doi:10.1016/j.actbio.2020.12.046
13. Qiu S, Xie L, Lu C, et al. Gastric cancer-derived exosomal miR-519a-3p promotes liver metastasis by inducing intrahepatic M2-like macrophage-mediated angiogenesis. *J Exp Clin Cancer Res*. 2022;41(1):296. doi:10.1186/s13046-022-02499-8
14. Wei S, Peng L, Yang J, et al. Exosomal transfer of miR-15b-3p enhances tumorigenesis and malignant transformation through the DYNLT1/Caspase-3/Caspase-9 signaling pathway in gastric cancer. *J Exp Clin Cancer Res*. 2020;39(1):32. doi:10.1186/s13046-019-1511-6
15. Xing H, Zhang Z, Mao Q, et al. Injectable exosome-functionalized extracellular matrix hydrogel for metabolism balance and pyroptosis regulation in intervertebral disc degeneration. *J Nanobiotechnology*. 2021;19(1):264. doi:10.1186/s12951-021-00991-5
16. Jiang T, Liu S, Wu Z, et al. ADSC-exo@MMP-PEG smart hydrogel promotes diabetic wound healing by optimizing cellular functions and relieving oxidative stress. *Mater Today Bio*. 2022;16:100365. doi:10.1016/j.mtbio.2022.100365
17. Liu Y, Lin S, Xu Z, et al. High-performance hydrogel-encapsulated engineered exosomes for supporting endoplasmic reticulum homeostasis and boosting diabetic bone regeneration. *Adv Sci*. 2024;11(17):e2309491. doi:10.1002/advs.202309491
18. Li Y, Bi D, Hu Z, Yang Y, Liu Y, Leung WK. Hydrogel-forming microneedles with applications in oral diseases management. *Materials*. 2023;16(13). doi:10.3390/ma16134805
19. Wang Z, Gao S, Zhang W, et al. Polyvinyl alcohol/chitosan composite hydrogels with sustained release of traditional Tibetan medicine for promoting chronic diabetic wound healing. *Biomater Sci*. 2021;9(10):3821–3829. doi:10.1039/d1bm00346a
20. Mohammadpour M, Samadian H, Moradi N, et al. Fabrication and characterization of nanocomposite hydrogel based on Alginate/Nano-Hydroxyapatite loaded with Linum *usitatissimum* extract as a bone tissue engineering scaffold. *Mar Drugs*. 2021;20(1):20. doi:10.3390/md20010020
21. Chenicheri S, Ramachandran R, Rajamanikam U. Antimicrobial effects of hydroxyapatite mosaicked polyvinyl alcohol-alginate semi-interpenetrating hydrogel-loaded with ethanolic extract of *Glycyrrhiza glabra* against oral pathogens. *Prog Biomater*. 2022;11(4):373–383. doi:10.1007/s40204-022-00199-2
22. Zhang Y, Zhang P, Gao X, Chang L, Chen Z, Mei X. Preparation of exosomes encapsulated nanohydrogel for accelerating wound healing of diabetic rats by promoting angiogenesis. *Mater Sci Eng C Mater Biol Appl*. 2021;120:111671. doi:10.1016/j.msec.2020.111671
23. Zhang L, Zhang Y, Miao M, et al. Erxian herbal pair enhances bone formation in infected bone nonunion models and attenuates lipopolysaccharide-induced osteoblastinhibition by regulating miRNA-34a-5p. *Bioengineered*. 2022;13(6):14339–14356. doi:10.1080/21655979.2022.2085388
24. Ren X, Liang Z, Zhao X. Preparation of hydroxyapatite nanofibers by using ionic liquids as template and application in enhancing hydrogel performance. *Front Bioeng Biotechnol*. 2023;11:1247448. doi:10.3389/fbioe.2023.1247448
25. Yan R, Guo Y, Wang X, Liang G, Yang A, Li J. Near-infrared light-controlled and real-time detection of osteogenic differentiation in mesenchymal stem cells by upconversion nanoparticles for osteoporosis therapy. *ACS Nano*. 2022;16(5):8399–8418. doi:10.1021/acsnano.2c02900
26. Abe T, Hajishengallis G. Optimization of the ligature-induced periodontitis model in mice. *J Immunol Methods*. 2013;394(1–2):49–54. doi:10.1016/j.jim.2013.05.002
27. Pereira SSC, Araujo GF, de Queiroz LN, et al. An alternative, easy and reproducible method of stabilization and ligature-induced periodontitis in mouse. *MethodsX*. 2019;6:2156–2165. doi:10.1016/j.mex.2019.09.004
28. Tamura H, Maekawa T, Hiyoshi T, Terao Y. Analysis of Experimental Ligature-Induced Periodontitis Model in Mice. *Methods mol Biol*. 2021;2210:237–250. doi:10.1007/978-1-0716-0939-2_23
29. Wang D, Li Q, Xiao C, Wang H, Dong S. Nanoparticles in periodontitis therapy: a review of the current situation. *Int J Nanomed*. 2024;19:6857–6893. doi:10.2147/ijn.S465089
30. Chen L, Zhu S, Guo S, Tian W. Mechanisms and clinical application potential of mesenchymal stem cells-derived extracellular vesicles in periodontal regeneration. *Stem Cell Res Ther*. 2023;14(1):26. doi:10.1186/s13287-023-03242-6
31. Zhang Y, Chen J, Fu H, et al. Exosomes derived from 3D-cultured MSCs improve therapeutic effects in periodontitis and experimental colitis and restore the Th17 cell/Treg balance in inflamed periodontium. *Int J Oral Sci*. 2021;13(1):43. doi:10.1038/s41368-021-00150-4
32. Shaikh MS, Shahzad Z, Tash EA, Janjua OS, Khan MI, Zafar MS. Human umbilical cord mesenchymal stem cells: current literature and role in periodontal regeneration. *Cells*. 2022;11(7):1168. doi:10.3390/cells11071168
33. Shareghi-Oskoue O, Aghebati-Maleki L, Yousefi M. Transplantation of human umbilical cord mesenchymal stem cells to treat premature ovarian failure. *Stem Cell Res Ther*. 2021;12(1):454. doi:10.1186/s13287-021-02529-w
34. Guo G, Tan Z, Liu Y, Shi F, She J. The therapeutic potential of stem cell-derived exosomes in the ulcerative colitis and colorectal cancer. *Stem Cell Res Ther*. 2022;13(1):138. doi:10.1186/s13287-022-02811-5
35. Mai Z, Chen H, Ye Y, et al. Translational and clinical applications of dental stem cell-derived exosomes. *Front Genet*. 2021;12:750990. doi:10.3389/fgene.2021.750990
36. El Baradie KBY, Nouh M, O'Brien III F, et al. Freeze-dried extracellular vesicles from adipose-derived stem cells prevent hypoxia-induced muscle cell injury. *Front Cell Dev Biol*. 2020;8:181. doi:10.3389/fcell.2020.00181
37. Peng W, Chang M, Wu Y, et al. Lyophilized powder of mesenchymal stem cell supernatant attenuates acute lung injury through the IL-6-p-STAT3-p63-JAG2 pathway. *Stem Cell Res Ther*. 2021;12(1):216. doi:10.1186/s13287-021-02276-y
38. Zhang Y, Bi J, Huang J, Tang Y, Du S, Li P. Exosome: a review of its classification, isolation techniques, storage, diagnostic and targeted therapy applications. *Int J Nanomed*. 2020;15:6917–6934. doi:10.2147/ijn.S264498
39. Zhao G, Lu G, Fan H, et al. Herbal products-powered thermosensitive hydrogel with phototherapy and microenvironment reconstruction for accelerating multidrug-resistant bacteria-infected wound healing. *Adv Healthc Mater*. 2024;13(15):e2400049. doi:10.1002/adhm.202400049
40. Wen B, Dai Y, Han X, et al. Biomineralization-inspired mineralized hydrogel promotes the repair and regeneration of dentin/bone hard tissue. *NPJ Regen Med*. 2023;8(1):11. doi:10.1038/s41536-023-00286-3
41. Abbaszadeh H, Ghorbani F, Derakhshani M, Movassaghpour A, Yousefi M. Human umbilical cord mesenchymal stem cell-derived extracellular vesicles: a novel therapeutic paradigm. *J Cell Physiol*. 2020;235(2):706–717. doi:10.1002/jcp.29004

42. Oveili E, Vafaei S, Bazavar H, et al. The potential use of mesenchymal stem cells-derived exosomes as microRNAs delivery systems in different diseases. *Cell Commun Signal*. 2023;21(1):20. doi:10.1186/s12964-022-01017-9
43. Ho PTB, Clark IM, Le LTT. MicroRNA-based diagnosis and therapy. *Int J mol Sci*. 2022;23(13):7167. doi:10.3390/ijms23137167
44. Sonkoly E, Ståhle M, Pivarcsi A. MicroRNAs and immunity: novel players in the regulation of normal immune function and inflammation. *Semin Cancer Biol*. 2008;18(2):131–140. doi:10.1016/j.semcancer.2008.01.005
45. Liu L, Guo S, Shi W, et al. Bone marrow mesenchymal stem cell-derived small extracellular vesicles promote periodontal regeneration. *Tissue Eng Part A*. 2021;27(13–14):962–976. doi:10.1089/ten.TEA.2020.0141
46. Rovas A, Puriene A, Snipaitiene K, et al. Analysis of periodontitis-associated miRNAs in gingival tissue, gingival crevicular fluid, saliva and blood plasma. *Arch Oral Biol*. 2021;126:105125. doi:10.1016/j.archoralbio.2021.105125
47. Nisha KJ, Janam P, Harshakumar K. Identification of a novel salivary biomarker miR-143-3p for periodontal diagnosis: a proof of concept study. *J Periodontol*. 2019;90(10):1149–1159. doi:10.1002/jper.18-0729
48. Roush S, Slack FJ. The let-7 family of microRNAs. *Trends Cell Biol*. 2008;18(10):505–516. doi:10.1016/j.tcb.2008.07.007
49. Liu P, Qin L, Liu C, et al. Exosomes derived from hypoxia-conditioned stem cells of human deciduous exfoliated teeth enhance angiogenesis via the transfer of let-7f-5p and miR-210-3p. *Front Cell Dev Biol*. 2022;10:879877. doi:10.3389/fcell.2022.879877
50. Shen GY, Ren H, Shang Q, et al. Let-7f-5p regulates TGFBR1 in glucocorticoid-inhibited osteoblast differentiation and ameliorates glucocorticoid-induced bone loss. *Int J Biol Sci*. 2019;15(10):2182–2197. doi:10.7150/ijbs.33490
51. Fu XF, Zhao HC, Yang CL, et al. MicroRNA-203-3p inhibits the proliferation, invasion and migration of pancreatic cancer cells by downregulating fibroblast growth factor 2. *Oncol Lett*. 2021;22(2):626. doi:10.3892/ol.2021.12887
52. Chen J, Xu Q, Zhang W, et al. MiR-203-3p inhibits the oxidative stress, inflammatory responses and apoptosis of mice podocytes induced by high glucose through regulating Sema3A expression. *Open Life Sci*. 2020;15(1):939–950. doi:10.1515/biol-2020-0088
53. Niu S, Xiang F, Jia H. Downregulation of lncRNA XIST promotes proliferation and differentiation, limits apoptosis of osteoblasts through regulating miR-203-3p/ZFPM2 axis. *Connect Tissue Res*. 2021;62(4):381–392. doi:10.1080/03008207.2020.1752200
54. Iwaszko M, Biały S, Bogunia-Kubik K. Significance of Interleukin (IL)-4 and IL-13 in Inflammatory Arthritis. *Cells*. 2021;10(11):3000. doi:10.3390/cells10113000
55. Krasnikov BF, Chien CH, Nostramo R, et al. Identification of the putative tumor suppressor Nit2 as omega-amidase, an enzyme metabolically linked to glutamine and asparagine transamination. *Biochimie*. 2009;91(9):1072–1080. doi:10.1016/j.biochi.2009.07.003
56. Lin CH, Chung MY, Chen WB, Chien CH. Growth inhibitory effect of the human NIT2 gene and its allelic imbalance in cancers. *Febs j*. 2007;274 (11):2946–2956. doi:10.1111/j.1742-4658.2007.05828.x
57. Chen X, Wan Z, Yang L, et al. Exosomes derived from reparative M2-like macrophages prevent bone loss in murine periodontitis models via IL-10 mRNA. *J Nanobiotechnology*. 2022;20(1):110. doi:10.1186/s12951-022-01314-y
58. Shen Z, Kuang S, Zhang Y, et al. Chitosan hydrogel incorporated with dental pulp stem cell-derived exosomes alleviates periodontitis in mice via a macrophage-dependent mechanism. *Bioact Mater*. 2020;5(4):1113–1126. doi:10.1016/j.bioactmat.2020.07.002